Track Electrostatic Model for Describing Secondary Ion Emission of Insulators

P. Iza, R. Sigaud, L.S. Farenzena, C.R. Ponciano, and E.F. da Silveira

Departamento de Física, Pontifícia Universidade Católica C.P. 38071, Rio de Janeiro 22452-970, Brazil

Received on 10 January, 2005

A model based on the nuclear track potential is described and used to predict trajectories and the energy distribution of secondary ions emitted by insulating targets. In this model, the electric field generated by each track pushes away the secondary ions formed on the target surface. The effects on the potential due to target thickness, track charge density, projectile incidence angle and secondary ion mass are analyzed. Predictions are compared with experimental data existing in the literature. It is found that the proposed model describes partially the behavior observed in the angular distribution of the emitted ions and new processes are proposed to be included in the model.

1. INTRODUCTION

Whenever a projectile with velocity comparable to the Bohr velocity penetrates a solid, it interacts mainly with the electrons of the target atoms. The projectile slows down at a rate very close to the value predicted by the electronic stopping power, transferring energy via inelastic collisions with electrons, i.e., electronic excitation or ionizations. In this process, the secondary electrons diffuse away from the track, crossing eventually the target surface, ionizing and desorbing surface atoms.

To describe the target modification or the secondary emission processes, a basic model - based on the track electrostatic potential - has been treated by several authors [1-5]. In this article, a Secondary Electron Induced Desorption - SEID model for insulating targets is discussed and used to calculate the secondary ion dynamics, particularly the desorbed ion trajectories and the kinetic energy distribution that those ions have after being accelerated in the region covered by the track potential. It is examined the dependence of the energy distributions on the model parameters: the projectile angle, the insulator thickness, the secondary ion mass and the track charge density (related to the projectile-target stopping power).

2. THE SEID MODEL

The basic processes and the geometry considered in the track potential model are represented in Fig. 1. The Z direction is set to be perpendicular to the target surface and the X direction lies along the surface, defining the projectile incidence plane ($y = 0$). The projectile goes towards negative values of z and x. The incidence angle is θ_p and the impact on the insulator target surface occurs at $x = y = z = 0$. The coordinates of the center of a given adsorbed molecule are x_0, y_0 and z_0. The distance z_0, typically equal to 1 Å, is considered to be the distance between the adsorbed molecule and the insulating layer. The projectile traverses the insulating layer of thickness L, producing a positively charged nuclear track of length $L_T = L/\cos\theta_p$, and a conducting substrate (necessary for the experiment) where the local track is promptly neutralized. The total charge of the track is $Q = n_e e L/\cos\theta_p$, where n_e is the number of secondary electrons produced by length

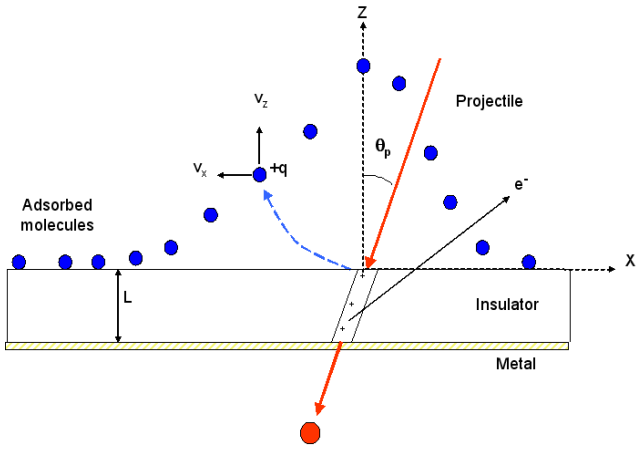

FIG. 1: Sketch of the geometry and processes involved in the phenomenon of induced ion desorption. The projectile traverses obliquely an insulating layer, producing a positive track and forcing a fraction of secondary electrons to cross the target surface. Adsorbed molecules are ionized by these electrons and are repelled from the surface by the track potential.

unit and e is the electron charge. It is supposed that this charge density remains constant during the ion desorption process, so that the track electric field is conservative.

The goals of the model are:

i) To calculate the number of desorbed ions per impact and per area unit, $N_{SI}(x_0, y_0)$, that leave the surface at the location x_0, y_0.

ii) To determine the trajectories of the desorbed ions.

iii) To determine the (final) energy and angular distributions of the desorbed ions, $N(E_f)$, i.e., after they have been accelerated by the track potential.

Analytical expressions

Considering $V = 0$ as the reference potential at an infinite distance of the track and neglecting polarization of the dielectric medium ($\varepsilon = \varepsilon_0$), the potential V_T at a point with coordinates x, y and z is:

$$V_T(x,y,z) = \frac{e}{4\pi\varepsilon_0}\int_0^{L_T} \frac{n_e(s)}{\sqrt{(x+s\sin\theta_p)^2+y^2+(z+s\cos\theta_p)^2}}\,ds \tag{1}$$

and the electric field at the same point is:

$$\vec{E}(x,y,z) = \frac{e}{4\pi\varepsilon_0}\int_0^{L_T} n_e \frac{(x+s\sin\theta_p)\,\hat{x}+y\hat{y}+(z+s\cos\theta_p)\,\hat{z}}{\left((x+s\sin\theta_p)^2+y^2+(z+s\cos\theta_p)^2\right)^{3/2}}\,ds \tag{2}$$

The model assumes no direct interaction between the projectile and adsorbed atoms or molecules. It is considered that only secondary electrons, produced by the projectile inside the insulator, ionize the adsorbed species. Defining $n(x_0,y_0)$ as the molecule density at the surface, $\bar{\sigma_e}$ as the average cross section of the adsorbed molecule by the secondary electron flux and P_i as the probability that this ionized molecule can desorb as an ion, the areal density of desorbed ions is:

$$N_{SI}(x_0,y_0) = \bar{\sigma_e} P_i\, n(x_0,y_0) \tag{3}$$

$$n(x_0,y_0) = \int_0^{L_T} n_e\, f_\Omega(x_0,y_0,s)\, e^{-l/\zeta} \tag{4}$$

where n_e is the number of secondary electrons (SE) produced in a track element of length ds. The fraction $f_\Omega(x_0,y_0,s)$ is $1/4\pi$ of the solid angle that an adsorbed molecule, located at the coordinates (x_0,y_0), is seen by the track element at the position s; l is the distance between this element and the molecule; ζ is the diffusion length of secondary electrons through the insulator, so that the integral of $n_e f_\Omega \exp(-l/\zeta)$ over the track represents the number of electrons coming from the track and reaching the molecule sitting on the target surface. The quantity n_e is obtained by dividing the electronic stopping power dE/ds by the average energy E_e transferred to each SE, i.e., the energy necessary to ionize the insulator atoms plus the SE average initial kinetic energy:

$$n_e = \frac{1}{E_e}\frac{dE_p}{ds} \tag{5}$$

The fraction f_Ω is given by

$$f_\Omega(x_0,y_0,s) = \frac{\pi R^2}{4\pi l^2} \tag{6}$$

where $l^2 = (x+s\sin\theta_p)^2+y^2+(z+s\cos\theta_p)^2$, $4\pi l^2$ is the area of a sphere with radius l and πR^2 is the apparent area of the adsorbed molecule sitting on this sphere.
The charge at the target surface just after the impact is

$$Q_s = e\int N_{SI}(x_0,y_0)\,dx_0\,dy_0 \tag{7}$$

The electron diffusion process is very complex because it depends on: a) the initial energy of the secondary electrons; b) the energy and recoiling direction of the produced tertiary electrons; c) the number of collisions that, on average, occur between the electron emission in the track and its arrival on the solid surface; and d) the SE capture in the bulk. In the beginning of the cascade process, energetic electrons (δ-electrons) are emitted forward, close to the projectile direction, while low energy electrons are emitted perpendicularly to the track. After a few electron-electron collisions, the direction of their movement becomes random and the secondary electron cloud starts to diffuse isotropically. However, such a complexity is not considered in the current version of the SEID model: tertiary electrons and surface barrier potential (the work function) are neglected and it has been assumed that the electrons are isotropically and monoenergetically emitted from the track. This picture gives rise to two tracks: the inner one, called infratrack, positively charged and whose diameter is typically the atomic diameter; and the outer one, called ultratrack, negatively charged and with an average radius approximately equal to ζ. Charge distributions and energy density distributions of both tracks have been discussed in the literature [5-10]. In the current electric field calculations, only the infratrack charge was used to determine V_T (see eq. 1). Since this electric potential is conservative, the desorbed ion's final energy (far way from the target) is given by $E_f = qV(x_0,y_0)+E_0$, where E_0 is the kinetic energy of the ion leaving the target and q is the ion's charge. Then, it is possible to combine eqs. 1 and 4 in order to get their energy distribution $N(E_f)$:

$$N(E_f) = \int_{dA(E_f)} N(x_0,y_0)\,dx_0\,dy_0 \tag{8}$$

where $dA(E_f)$ is the elemental area, on the target surface, between the equipotentials corresponding to $E_f - E_0$ and $E_f - E_0 + dE_f$.

Once the electric field (eq. 2) over the whole space and the initial position of the ions on the surface (eq. 4) are known, 2^{nd} Newton Law can be applied to determine trajectories and velocities. Considering n_e constant, the integral of eq. 2 can be performed analytically. The Verlet algorithm [11] is convenient to solve the equation of motion iteratively.

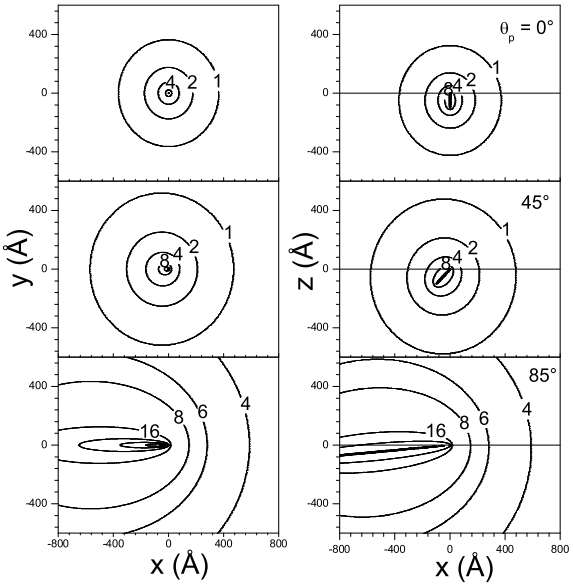

FIG. 2: Equipotentials of the track field, for different incidence angles, :a) on the target surface (left) and b) in the projectile incidence plane (right). Note that the target thickness is kept constant ($L = 100$Å), so that the track length increases with θ_p. The maximum potential (V_{max}) is indicated.

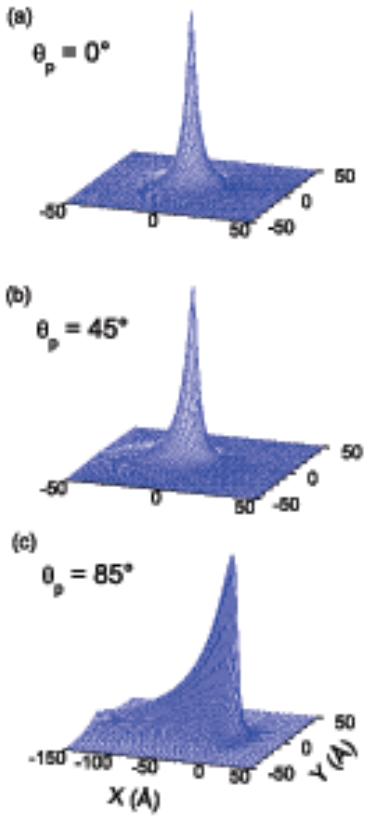

FIG. 3: The areal density of ionized adsorbed molecules for $\theta_p = 0°$, 45° and 85°. The value of the distribution $n(x_0,y_0)$ and its coordinate x_{max} are displayed.

3. NUMERICAL PREDICTIONS OF THE MODEL

3.1. Equipotentials of the projectile track electric field

Once the positively charged track is formed in the insulator, an electric field with cylindrical symmetry (eq. 1) appears around the track. The obtained equipotentials over the XY and XZ planes (top and lateral views, respectively) are displayed in Fig. 2 for three incidence angles: $\theta_p = 0°$, 45° and 85°. Calculation was performed for an insulator thickness of $L = 100$ Å, and for a track linear charge density of $n_e e = 0.1e/$Å (value suggested by Moshammer et al. [12]).

One sees clearly that increasing the incidence angle, the electric potential increases (the total charge Q in the track increases with $\cos^{-1}\theta_p$) and that the maximum potential on the XY plane (which defines the solid surface) occurs at the impact point $x = y = 0$. A specular symmetry always exists with respect to the incidence plane: $V_T(x,-y,z) = V_T(x,y,z)$ and, obviously, for $\theta_p = 0°$ a cylindrical symmetry around the normal direction to the surface appears. It is seen in the plots that, even for non zero incidence angle, a cylindrical symmetry appears around the track. Actually this incorrect behavior is due to the consideration in eq. 1 that $\varepsilon = \varepsilon_0$ inside the insulator and also to the fact that charge images produced by the metallic substrate are neglected.

3.2. Surface charge density

The secondary electron flux through the surface ionizes adsorbed molecules. The surface (areal) charge density $N_{SI}(x_0,y_0)$ is considered proportional to this flux and is calculated by making use of eqs. (4-6). Fig. 3 illustrates how the function $N_{SI}(x_0,y_0)$ changes with the incidence angle. $L = 100$ Å, $R = 0.8$ Å, $n_e e = 0.1$Å^{-1} and the diffusion length $\zeta = 20$ Å have been considered. For $\theta_p = 0°$, a symmetrical function $N_{SI}(x_0,y_0)$ is found and the ionized region around the impact point is a circle with a diameter close to 2Å. A small asymmetry is seen for $\theta_p = 45°$, while the grazing impact ($\theta_p = 85°$) produces ionized strip having a ~ 2Å width and $\sim (L/\cos\theta_p)$ long. The total ion charge on the surface should present roughly the same dependence $\cos^{-1}\theta_p$ as Q does.

Table I gives numerical results obtained from the model's expressions.

Note that the charge density at the impact site does not change substantially with θ_p. The $N_{SI}(x_0,y_0)$ maximum value moves towards negative x (the track side) when θ_p increases.

θ_p	$N_{SI}(0,0)$	$N_{SI}^{max}(x_{max},0)$	x_{max}(Å)	$V_{max}(V)$	$Q_s(e)$
0°	0.466	0.466	0.0	18	96.0
45°	0.498	0.551	-1.0	20	131
85°	0.582	0.969	-5.0	36	973

TABLE I: Predicted charge densities, maximum values of surface potentials and total surface charge for three incidence angles: $\theta_p = 0°$, 45° and 85°. $N_{SI}(0,0)$ is the secondary ion density at the impact point. V_{max} is the electric potential at x_{max}, the coordinate corresponding to the maximum value of N_{SI}. Q_S is calculated considering $\bar{\sigma_e} P_i = 1$.

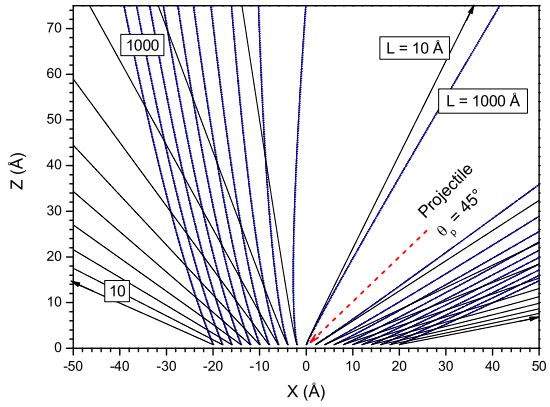

FIG. 4: Trajectories of H^+ secondary ions for a projectile impinging at $\theta_p = 45°$. Two target thickness are considered: $L = 10$ Å and 1000 Å, solid and dash lines respectively.

3.3. The desorbed ion motion

The majority of the ions formed from adsorbed molecules hit by secondary electrons probably is neutralized on the surface and does not desorb or desorb as neutrals. Some surface positive ions are ejected and accelerated by the track repulsive electric field. In order to make clear the effect of the track potential on desorbed ion motion, it is assumed that: a) the emission occurs with zero initial velocity; b) the electric fields produced by the surface ions and by external sources are negligible, i.e. , only the charged track is source of the electric potential (see 3.1).
Hydrogen ions, for their constant presence in desorption experiments were selected for illustrate the model predictions. Results are presented in Fig. 4 for two target layer thicknesses ($L = 10$ Å and 1000 Å, solid and dashed lines respectively). The projectile impinges at $\theta_p = 45°$, producing therefore track lengths of 14 and 1400 Å (both having $n_e = 0.1$ Å^{-1}). The H^+ ions, placed each 2 Å along the X axis, leave the target surface in the incidence plane.

The following characteristics are extracted from the calculations.
Geometrical properties: a) trajectories close to the projectile direction are relatively rare, i.e., the angular distribution has roughly a *crater shape* produced by ions running close to a conical surface coaxial to the projectile beam direction; b) ion dispersion for positive x is lower than for negative x; c) the larger the track, the closer the ion emission to the projectile direction - or inversely - very short track tends to produce isotropic ion emission.

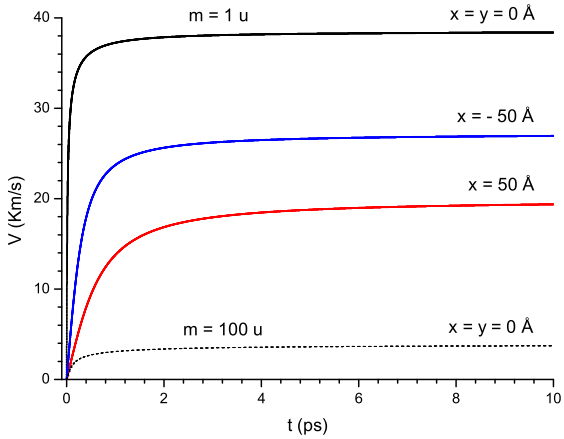

FIG. 5: Dependence of the secondary ion total velocity on the desorption time. Solid lines correspond to $m = 1u$ secondary ion and dash line to a $m = 100u$ ion.

Dynamics (Fig. 5): a) ions emitted from the impact site ($x = y = 0$) have the highest final velocity; b) ions emitted from the negative x have higher velocity than the correspondent positive x; c) the final velocity is proportional to the inverse of the square root of the ion mass (since the final kinetic energies are the same) and d) the lower the mass, the faster the ion attains its final velocity (as this potential is conservative). The dashed line represents the velocity of an ion with m = 100 u as function of the desorption time; the final velocity is 10 times lower than an m = 1 u ion desorbed from the same spot.

3.4. Angular distribution

Fig. 6 shows - for the three incidence angles considered - the x y coordinates ($y > 0$) of desorbed ions in three different times of their movement: a) $t = 0$, i.e., $z = z_0$, when the ions are about to leave the target surface plane; b) $t = t_f$, when the track repulsive force becomes negligible ($t_f = 10$ ps for the current calculation); and c) $z = z_{det}$, when the ions arrive at the detector surface. The target thickness is $L = 100$ Å for all cases. For the planes $z = z_0$ and $z = z_{det}$, the density of points is proportional to the density of trajectories crossing each plane; for $t = t_f$, as the ions are distributed over different z positions it is plotted their projection into the XY plane. Note that the projected x and y dimensions are: Å for the first two columns projected on target and cm for the third projected detector. For the latter situation, it is considered that the acceleration region of the ions is 0.71 cm, the acceleration potential

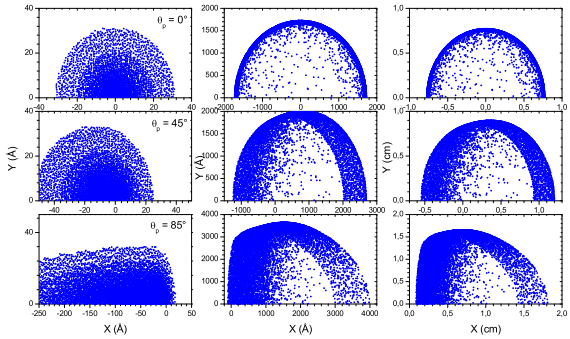

FIG. 6: Predicted XY projected distribution for $\theta_p = 0°$, 45° and 85° at different desorption times. Left: on the target surface; center: after $t = 10$ ps; right: on the detector surface. Note the strong repulsion of the ions when they desorb close to the impact spot.

is $V_{acc} = 4.0\,kV$ and the drift region is 37 cm long. Since the external acceleration field is axial, the x-y radial dispersion is due uniquely to the track radial field component. As expected, for $\theta_p = 0°$, the point distribution has a rotational symmetry over all the three planes. The crater shape, characteristic of the track potential repulsion, is seen in the z_f and plane distributions. The crater becomes asymmetric for $\theta_p = 45°$ and its center moves towards positive x. For $\theta_p = 85°$, this effect is more pronounced.

3.5. Energy distributions

Particular energy distributions may be defined for the desorbed ions: one at the target surface, $N(E_0)$, another when local forces vanish, $N(E_f)$, and another at the detector surface, $N(E_{det})$, after the action of external forces. In this work it is considered $N(E_0) = 0$ for all ions. $N(E_f)$ can be determined either by eq. 8 or by solving the equation of motion (Verlet method). $N(E_{det})$ can be easily deduced from $N(E_f)$ by using $E_f = E_0 + qV_{acc}$. It should be reminded that experimental data obtained from standard time-of-flight give only the axial final velocity distributions, which in turn give "axial" and not "axial + radial" kinetic energy distribution. Therefore, in order to compare predictions with usual experimental data, the ion dynamics need to be solved.

Fig. 7 shows the axial (low) and the total (up) energy distributions, respectively, predicted by the model. Calculations were done for $L = 100$ Å, $n_e = 0.1$ Å^{-1}, $\theta_p = 0°$, 45° and 85°.

4. COMPARISON WITH EXPERIMENT

Secondary H^+ ion emission has been analyzed by many groups [1,13-15]. In particular, Most et al. [13] and Jalowy et al. [14] have measured XY distributions and found that they are emitted asymmetricaly, most of the H^+ against the incoming beam. This agrees with the results shown in Fig. 6: the

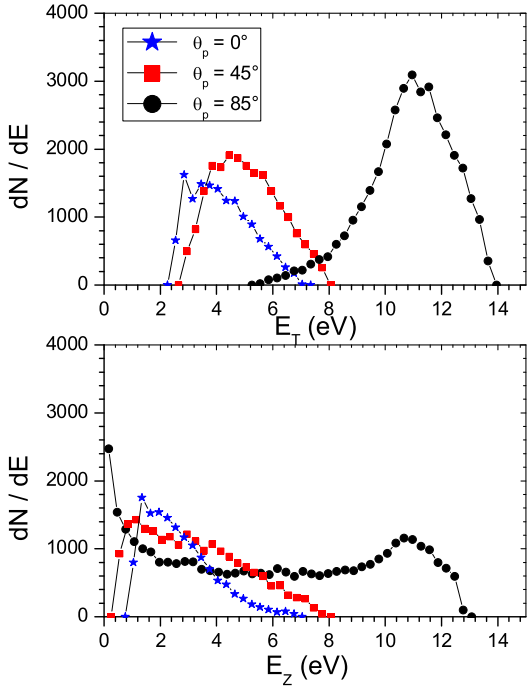

FIG. 7: Total (upper graph) and axial (lower graph) energy distributions given by the model. Calculations were done for $L = 100$ Å, $n_e e = 0.1\,e$/Å, $\theta_p = 0°$, 45° and 85°

more grazing the impact is, the more backwards the secondary ions are emitted. On the other hand, the crater shape predicted by the SEID model is not observed experimentally, indicating that either the $N_{SI}(x_0, y_0)$ function is higher near the impact spot or the hypothesis that SI are emitted with non zero initial velocity reduces the crater effect.

5. CONCLUSIONS

Secondary electrons diffuse inside the solid up to its surface, where they ionize and induce adsorbed molecules to desorb. This work proposes a model to describe the dynamics of the surface ion formation and emission. The influence of each parameter of the model on the angular and energy distributions of the emitted ions is discussed. Comparison with experimental data indicates partial qualitative agreement, so improvements in the model are necessary in order to enhance the H^+ emission close to the track direction.

It is suggested, based on eq. 4, that P_i : a) should be maximum at $x_0 = y_0 = 0$, where the positive track cannot furnish electrons to neutralize the adsorbed ions and b) should increase with their initial velocity. The second suggestion comes from the fact that the higher is the SI velocity, the lower is the probability that the SI could be neutralized.

Acknowledgments

CNPq, FAPERJ and CLAF are gratefully acknowledged for partial support of this research.

[1] K. Wien, Ch. Kock and Nguyen Van Tan, Nucl. Instr. and . Meth. in Phys. Res. B **100**, 322 (1995).
[2] G. Schiwietz, P. L. Grande, B. Skogwall, J.P. Biersack, R. Köhrbrück, K. Sommer, A. Schmoldt, P. Goppelt, I. Kádár, S. Ricz, and U. Stettner, Phys. Rev. Lett. **69**, 628 (1992).
[3] H. Rothard, C. Caraby, A. Cassimi, B. Gervais, J.P. Grandin, P. Jardin, M. Jung, A. Billebaud, M. Chevalier, K.O. Groeneveld, and R. Maier, Phys. Rev. A **51**, 3066 (1995).
[4] K. Kimura, S. Usui, and K. Nakajima, Phys. Rev. A **62**, 062902 (2000).
[5] P. Håkansson, Mat. Fys. Medd. Dan. Vidensk. Selsk. **43**, 593 (1993).
[6] D. Fenÿo, P. Håkansson, and B. U. R. Sundqvist, Nucl. Instrum. and Meth. in Phys. Res. B **84**, 31 (1994).
[7] B. U. R. Sundqvist, Int. J. Mass. Spectrom. Ion Processes **126**, 1 (1993).
[8] J. A. M. Pereira and E. F. da Silveira, Phys. Rev. Lett. **84**, 5904 (2000).
[9] C. C. de Castro, I. S. Bitensky, E. F. da Silveira, M. Most, and K. Wien Int. J. Mass Spectrom. and Ion Processes **173**, 1 (1998).
[10] R. M. Papaléo, P.Demirev, J. Eriksson, P. Håkansson, and B. U. R. Sundqvist, Phys. Rev. B **54**, 3173 (1997).
[11] L. Verlet, Phys. Rev. **159**, 98 (1967).
[12] R. Moshammer, R.Matthäus, K. Wien, Y. LeBeyec, and G. Bolbach, Technische Hochschule Darmstadt internal report, IKDA 89/36 (1989).
[13] M. Most, K. Wien, A. Brunelle, S. Della Negra, J. Depauw, D. Jacquet, M. Pautrat, and Y. LeBeyec, Nucl. Instr. and Meth. in Phys. Res. B **168**, 203 (2000).
[14] T. Jalowy, L. S. Farenzena, M. Hattass, E. F. da Silveira, H. Schmidt-Böcking, and K. O. Groeneveld, Nucl. Instr. and Meth. in Phys. Research B **22**, 78 (2004).
[15] G. Betz and K. Wien, Int. J. Mass Spectrom. and Ion Processes **140**, 1 (1994).